

Acoustic excitation of superharmonic capillary waves on a meniscus in a planar microgeometry

Jie Xu and Daniel Attinger

Laboratory for Microscale Transport Phenomena, Department of Mechanical Engineering, Columbia University, New York, New York 10027, USA

(Received 22 January 2007; accepted 6 September 2007; published online 18 October 2007)

The effects of ultrasound on the dynamics of an air-water meniscus in a planar microgeometry are investigated experimentally. The sonicated meniscus exhibits harmonic traveling waves or standing waves, the latter corresponding to a higher ultrasound level. Standing capillary waves with subharmonic and superharmonic frequencies are also observed, and are explained in the framework of parametric resonance theory, using the Mathieu equation. © 2007 American Institute of Physics. [DOI: 10.1063/1.2790968]

Instabilities at a liquid-gas interface appear in a wide range of physical systems, from large ocean waves to microscopic oscillations of a cavitating bubble.^{1,2} For a linear and conservative system the response is harmonic; i.e., with the same frequency as the excitation frequency.³ However, in 1831, Faraday observed⁴ the subharmonic response of a liquid-gas interface excited by vertical oscillations: the response frequency was half that of the excitation.⁵ Faraday waves are caused by the excitation of the gravity term of their eigenfrequency.⁵ This phenomenon can be explained by a Mathieu equation,⁴ and has been widely used to generate waves in large systems^{2,4,6,7} At smaller scale, gravity is negligible, and ultrasound is therefore more efficient for exciting waves. Using ultrasound, subharmonic responses have been observed^{8–10} on millimeter-size bubbles, a phenomenon relevant for bubble sizing,⁸ cavitation control,⁹ and acoustic streaming.¹⁰ Although the possibility of superharmonic response at a liquid-gas interface has been theoretically demonstrated,^{11–14} and superharmonic noise was recorded from a bubble cloud during a sonoluminescence study, no superharmonic wave at a liquid-gas interface has ever been directly observed. The occurrence of superharmonic waves was also qualified¹³ as improbable because of the higher damping associated with higher frequencies. In our study, we excite, with ultrasound, a liquid-gas meniscus pinned at the junction between a microchannel and a chamber, in a microfluidic chip. We observe superharmonic oscillations at the meniscus, as well as harmonic and subharmonic oscillations. These phenomena are described and explained in the framework of parametric resonance theory.

A typical microfluidic chip used in our study is shown in Fig. 1(a): it involves a chamber (E) fed by a forklike network of four channels, i.e., A, B, C, and D, with respective widths of 400, 1000, 400, and 100 μm . The height of each microchannel is 50 μm . The microfluidic chip is manufactured in polydimethylsiloxane (PDMS) using the soft lithography process described in Ref. 15. The PDMS chip is covered with a PDMS plate and sandwiched between two glass slides. This type of assembly ensures that every channel wall is made of PDMS, for the consistency of surface properties. A piezoelectric actuator is embedded in the PDMS cover

plate on top of chamber E to generate pressure waves in water. A stable air-water interface is then generated at the junction of channel D and the chamber by filling the chamber with water and then injecting air in channel D. Note in Fig. 1(b) that two microgeometrical features enhance the stability of the air-water interface.¹⁶ The piezoelectric actuator is driven by a function generator (Agilent, 33120A) and by a voltage amplifier (Krohn-Hite, 7600 M), at frequencies up to 300 kHz. Visualization is performed with a long-distance microscope in the plane perpendicular to the microfluidic chip, with a spatial resolution of 1 μm . A strobe microscopy technique is used for freezing the meniscus shape.¹⁷ A frequency divider is used between the function generator and the strobe diode, so that the diode frequency can be set to either the actuator frequency or half of its value, allowing the observation of superharmonic and subharmonic oscillations corresponding to half-integer multiples of the excitation frequency. Deionized water is used in the experiments. The physical properties used in this study are described in Table I. The surface tension, density, and viscosity are obtained from Ref. 18. The contact angles are measured from the microscopy pictures.

In our experiments, the piezoelectric transducer induces pressure oscillations in the water with a frequency f_e , which excite interfacial waves at a frequency f_1 . For relatively low excitation intensities and $100 \text{ kHz} < f_e < 170 \text{ kHz}$, we observed waves traveling on the meniscus surface at a frequency $f_1 = f_e$. Figure 2 shows a sequence taken at $f_e = 150 \text{ kHz}$, with a delay of 2 μs between each frame.

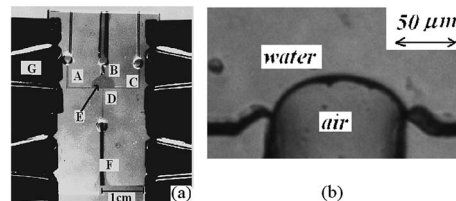


FIG. 1. (a) The microfluidic chip involves a chamber fed by a forklike network of four channels. Reprinted with permission from Ref. 16. © 2007 Institute of Physics. (b) Detail of the meniscus. Triangular microfeatures pin the meniscus wetting line.

TABLE I. Physical properties.

Symbol	Physical property	Value
σ	Surface tension of water	72.0 mN/m at 25 °C
		69.6 mN/m at 40 °C
ρ	Density of water	0.998 g/cm ³
θ	Contact angle of water on PDMS	70°, receding
		110°, advancing

Crests A and B are moving symmetrically towards the center of the channel, where they meet each other. This phenomenon occurs with the meniscus assuming either a curved shape (as in Fig. 2) or a flat shape (as in Fig. 5). Assuming conservative uncertainties $\Delta\lambda$ of $\pm 2 \mu\text{m}$ for the wavelength, the observed wavelengths and oscillation frequencies are plotted in Fig. 3. Since the wavelengths are small ($\lambda \ll 2\pi\kappa^{-1}$, where κ^{-1} is the water-air capillary length, with $2\pi\kappa^{-1}$ typically on the order of a centimeter), gravity can be neglected in the theoretical analysis: very likely, these waves are capillary waves, caused by joint effect of inertia and surface tension.

In a two-dimensional (2D) case, neglecting dissipative effects, the relationship between the wavelength and the oscillation frequency f_0 is given by the dispersion equation¹⁹ $\lambda_0 = [2\pi\sigma / (f_0^2\rho)]^{1/3}$. This relation is plotted in Fig. 3, for a water surface tension at the value of 40 °C, corresponding to the measured water temperature, slightly heated by resistive dissipation in the piezoelectric transducer. The relatively good agreement in Fig. 3 between the experimental data and the 2D theory can be justified by the fact that the curvature in the observation plane (radius on the order of 10 μm) is much larger than the curvature in the perpendicular plane (radius on the order of 80 μm). It appears, therefore, that the proposed microchannel/chamber configuration provides a simplified 2D model platform to observe wave at liquid-gas surfaces, without the complexity of configurations such as oscillating three-dimensional (3D) bubbles in an unbounded fluid.^{9,20}

Increasing the actuation intensity—while keeping the excitation frequency f_e constant at 150 kHz—generates a standing wave, which is described by the successive frames in Fig. 4. The standing wave has a larger amplitude (around 5 μm) than the traveling wave (around 2 μm ; see Fig. 2). In addition, in the case of Fig. 4, the frequency of the standing wave $f_1 = 1/2f_e$ is a subharmonic of the excitation frequency f_e . This phenomenon is also observed for a flat meniscus

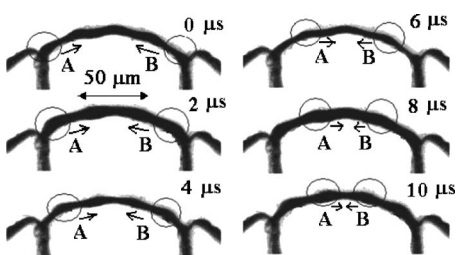


FIG. 2. Traveling waves on meniscus at 150 kHz (enhanced online).

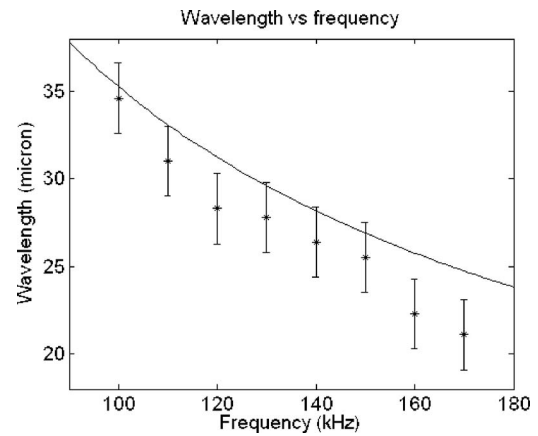


FIG. 3. Wavelength vs wave frequency. Reprinted with permission from Ref. 16. © 2007 Institute of Physics.

(Fig. 5). Typical experimental conditions with the threshold voltage above which standing waves replace traveling waves are given in Table II. Traveling waves are always harmonic at the excitation frequency f_e , while standing waves have a frequency f_1 that can be either subharmonic, harmonic, or superharmonic. For standing waves on a meniscus of length L fixed on two lateral walls, the allowable wavelengths are $\lambda = L/(n+1)$, where L and n are, respectively, the channel width and a positive integer.²¹ Figure 5 shows that the system spontaneously selects $n=1$.

The occurrence of subharmonic and superharmonic waves can be explained as the result of parametric oscillations. Let us express a standing wave as the superposition of two waves traveling in opposite directions:

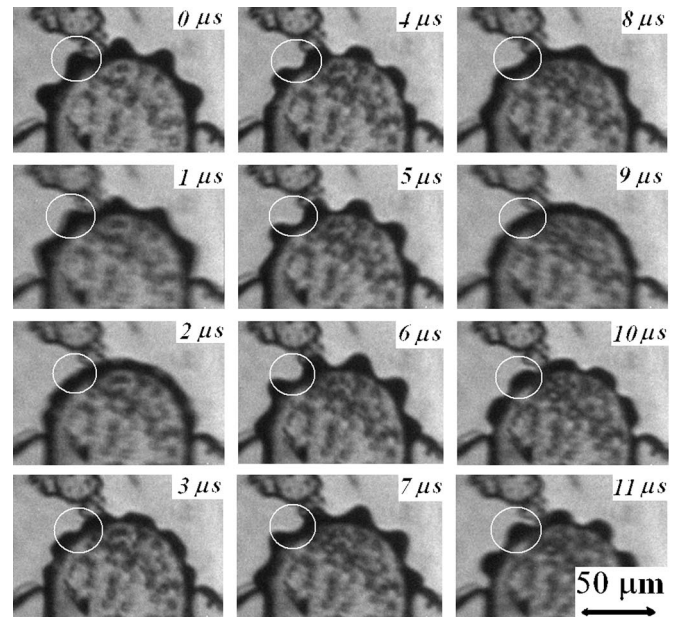


FIG. 4. Standing waves on meniscus interface excited at 150 kHz. The standing waves oscillate at 75 kHz. Note some condensation occurring along the walls of the air channel, a phenomenon found more often in the standing wave case than the traveling wave case. Reprinted with permission from Ref. 16. © 2007 Institute of Physics (enhanced online).

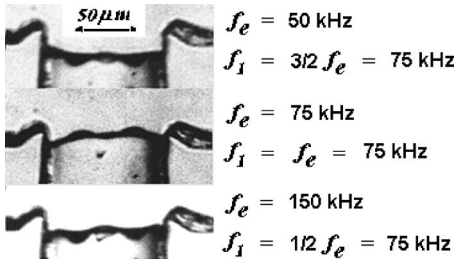


FIG. 5. Standing waves at different frequencies. Reprinted with permission from Ref. 16. © 2007 Institute of Physics.

$$\begin{aligned} \eta &= a \cos(2\pi x/\lambda - \omega t) + a \cos(2\pi x/\lambda + \omega t) \\ &= 2a \cos(2\pi x/\lambda) \cos(\omega t). \end{aligned} \quad (1)$$

The resulting surface displacement therefore both obeys the wave equation and the oscillator equation, the latter being of the general form (neglecting damping) $\ddot{\eta} + \omega^2 \eta = 0$. Figure 6 describes the wave and reference frame in two planes, the top one parallel to the chip surface and the bottom one perpendicular to it, with the x - z plane parallel to the chip surface.

Assuming the motion is only in the x - z plane and the flow is irrotational, the velocity potential ϕ can be found by solving the Laplace equation $\nabla^2 \phi = 0$, with zero velocity boundary condition at infinity and a kinematic boundary condition on the meniscus:

$$u = \frac{\partial \phi}{\partial x} = 0 \quad w = \frac{\partial \phi}{\partial z} = 0 \quad \text{at } z = \infty, \quad (2)$$

$$\frac{\partial \eta}{\partial t} = \frac{\partial \phi}{\partial z} \text{ at } z = 0. \quad (3)$$

In addition, a dynamic boundary condition arises from the Laplace pressure $\Delta P = \sigma(1/R_h + 1/R_w)$ across the meniscus interface, where the curvature radii are calculated from the 3D meniscus shape shown in Fig. 6:

$$\frac{1}{R_w} = \frac{-\partial^2 \eta / \partial x^2}{[1 + (\partial \eta / \partial x)^2]^{3/2}} \approx -\frac{\partial^2 \eta}{\partial x^2} \quad (4)$$

and

TABLE II. Critical voltages where the transition from traveling waves to standing waves occurs.

f_e (kHz)	f_1/f_e	f_1 (kHz)	Voltage (V)
175	1/2	87.5	98.6
150	1/2	75	29.9
127	1/2	63.5	77.4
75	1	75	182.8
74	1	74	182.3
50	3/2	75	107.7
49	3/2	73.5	95.1

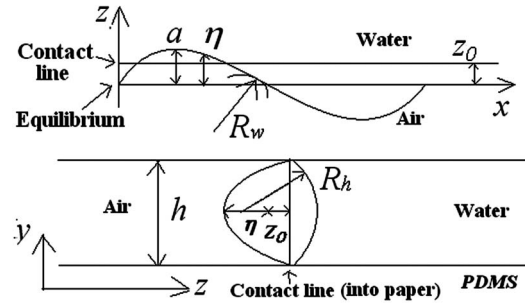


FIG. 6. Three-dimensional shape of the meniscus oscillation, where z_0 is the distance between contact line and the z location corresponding to $\eta=0$. Reprinted with permission from Ref. 16. © 2007 Institute of Physics.

$$\frac{1}{R_h} = \frac{2(\eta - z_0)}{(\eta - z_0)^2 + h^2/4}. \quad (5)$$

In the above equation, z_0 is defined in the caption of Fig. 6. For irrotational flow, the linearized Bernoulli equation $\partial \phi / \partial t + p/\rho = 0$ is applicable and can be combined with the Laplace boundary condition to give a third boundary condition

$$\rho \frac{\partial \phi}{\partial t} = \sigma \left(\frac{1}{R_h} + \frac{1}{R_w} \right) \text{ at } z = 0. \quad (6)$$

Solving $\nabla^2 \phi = 0$ with boundary conditions (2), (3), and (6) and assuming $z_0 = 0$ gives a modified dispersion equation between the wavelength λ and frequency f :

$$f^2 = \frac{\sigma}{\pi \rho \lambda^3} \left(2\pi^2 + \frac{4\lambda^2}{h^2} \right). \quad (7)$$

Inserting Eq. (7) into $\ddot{\eta} + \omega^2 \eta = 0$, we obtain

$$\ddot{\eta} + \frac{16\pi\sigma}{\lambda\rho} \left(\frac{\pi^2}{2\lambda^2} + \frac{1}{h^2} \right) \eta = 0. \quad (8)$$

It is reasonable to assume that the chamber height h is deforming with the piezoelectric deformation, with a small amplitude Δh at the excitation frequency f_e . In that case, we can write $h = h_0 + \Delta h \cos(\omega_e t)$ in Eq. (8). Neglecting second-order terms, we obtain

$$\ddot{\eta} + \frac{16\pi\sigma}{\lambda\rho} \left(\frac{\pi^2}{2\lambda^2} + \frac{1}{h_0^2} - \frac{2\Delta h}{h_0^3} \cos(\omega_e t) \right) \eta = 0, \quad (9)$$

which is a Mathieu equation²² representing a parametrically excited oscillator. Although this equation cannot be solved analytically, the boundaries between stable and unstable solutions can be analytically determined using the formulas in Ref. 22 and are shown in Fig. 7. Figure 7 shows, for a case in which damping is negligible, the zones of stability and instability, the latter being shown by thin lines that correspond to the bottom of Mathieu tongues. States in the instability zones correspond to the possibility of standing waves, as shown in Ref. 11. In the above derivation, the natural oscillation pulsation ω_0 of our system was identified as the pulsation ω_1 of the harmonic standing wave observed in Table II, which corresponds to the $f_1 = 75$ kHz case. The displacement Δh of the microchannel height is measured as the piezoelectric trans-

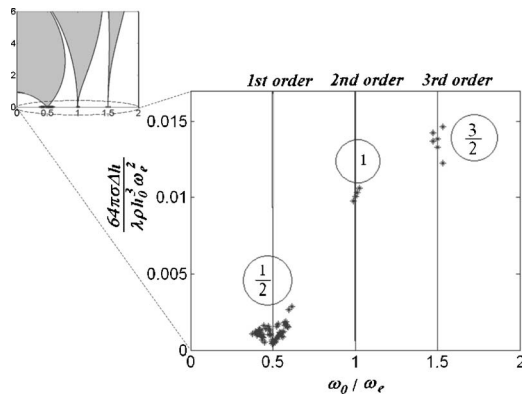


FIG. 7. Instability analysis of Eq. (9). The top left figure shows three instability zones in gray, known as Mathieu tongues. The bottom right figure shows thin lines that correspond to the bottom of Mathieu tongues, with our experimental data as stars. The circled numbers near the data points equal the ratio of wave frequencies over excitation frequencies f_1/f_e .

ducer deformation using atomic force microscopy, to be on the order of 200 nm. In Fig. 7, we have reported groups of experimental data wherein the transition from traveling to standing waves is observed during the process of slowly increasing the excitation frequency. The experimental points are gathered around the bottom of the three instability zones, with groups of frequency ratios corresponding to the ones predicted by the Mathieu equation. In Fig. 7, all the measured points close to the first-order zone have $f_1/f_e=1/2$ (subharmonic response), while the points close to the second- and third-order zones have f_1/f_e equal, respectively, to 1 (harmonic) and $3/2$ (superharmonic), as predicted theoretically.^{13,22} Figure 7 shows points close to the tongue boundaries, but not inside the tongues as was predicted by the derivation above. This can possibly be explained by non-idealities in the experimental setup, as follows. The natural pulsation ω_0 of our experimental system might experience slight variations over the duration of our study because (a) the system is made of a rubberlike material that deforms easily, (b) the actuator is heating the system, and (c) the shape and position of the meniscus and wetting angle vary slightly between each measurement. However, all the points in Fig. 7 are plotted assuming a unique natural pulsation ω_0 , as stated above. In other words, it is highly possible that an experiment done in a more controlled geometry would produce experimental points that fall exactly inside the Mathieu tongues and fully satisfy our theory. In Fig. 7, the points corresponding to higher-order standing waves are higher on the vertical scale, which might be due to high order nonlinear damping. For instance, it has been shown²³ that adding viscous damping to the Mathieu treatment pulls the Mathieu tongues upwards. In any case, the general trend revealed by our experiments in Fig. 7 is that instability states of order higher than $1/2$ are more difficult to produce than the $1/2$ -order instability state. This might explain why subharmonic oscillations are easier to observe at a liquid-gas interface.

In summary, the response of a water-air meniscus to ultrasonic excitation has been studied. When the excitation is

weak, traveling waves are found. When the excitation becomes stronger, standing waves appear at the meniscus interface. The ratio of the wave frequencies over the excitation frequencies assumes half integer values such as $1/2$, 1 , and $3/2$, a phenomenon explained by the Mathieu equation.

We thank the U.S. National Science Foundation for their support through the CAREER Grant No. 0449269. We thank Howard Stone (Harvard) and Michael Weinstein (Columbia APAM) for valuable suggestions.

- ¹T. G. Leighton, "From seas to surgeries from babbling brooks to baby scans: the acoustics of gas bubbles in liquids," *Int. J. Mod. Phys. B* **18**, 3267 (2004).
- ²M. Perlin and W. W. Schultz, "Capillary effects on surface waves," *Annu. Rev. Fluid Mech.* **32**, 241 (2000).
- ³J. P. D. Hartog, *Mechanical Vibrations* (McGraw-Hill, New York, 1947).
- ⁴J. Miles and D. Henderson, "Parametrically forced surface waves," *Annu. Rev. Fluid Mech.* **22**, 143 (1990).
- ⁵S. Douady, "Experimental study of the Faraday instability," *J. Fluid Mech.* **221**, 383 (1990).
- ⁶W. W. Schultz, J.-M. Vanden-Broeck, L. Jiang, and M. Perlin, "Highly nonlinear standing water waves with small capillary effect," *J. Fluid Mech.* **369**, 253 (1998).
- ⁷W. S. Edwards and S. Fauve, "Patterns and quasi-patterns in the Faraday experiment," *J. Fluid Mech.* **278**, 123 (1994).
- ⁸A. D. Phelps and T. G. Leighton, "High-resolution bubble sizing through detection of the subharmonic response with a two-frequency excitation technique," *J. Acoust. Soc. Am.* **99**, 1985 (1996).
- ⁹M. Sato, N. Shibuya, N. Okada, T. Tou, and T. Fujii, "Oscillation mode conversion and energy confinement of acoustically agitated bubbles," *Phys. Rev. E* **65**, 046302 (2002).
- ¹⁰M. Sato and T. Fujii, "Quantum mechanical representation of acoustic streaming and acoustic radiation pressure," *Phys. Rev. E* **64**, 026311 (2001).
- ¹¹T. B. Benjamin and F. Ursell, "The stability of the plane free surface of a liquid in vertical periodic motion," *Proc. R. Soc. London, Ser. A*, **225**, 505 (1954).
- ¹²S. J. Hogan, "The superharmonic normal mode instabilities of nonlinear deep-water capillary waves," *J. Fluid Mech.* **190**, 165 (1988).
- ¹³W. Eisenmenger, "Dynamic properties of the surface tension of water and aqueous solutions of surface active agents with standing capillary waves in the frequency range from 10 kc/s to 1.5 Mc/s," *Acustica* **9**, 327 (1959).
- ¹⁴M. S. Plesset, "Bubble dynamics and cavitation," *Annu. Rev. Fluid Mech.* **9**, 145 (1977).
- ¹⁵Y. Xia and G. M. Whitesides, "Soft lithography," *Angew. Chem., Int. Ed.* **37**, 550 (1998).
- ¹⁶J. Xu and D. Attinger, "Control and ultrasonic actuation of a gas-liquid interface in a microfluidic chip," *J. Micromech. Microeng.* **17**, 609 (2007).
- ¹⁷D. Attinger, Z. Zhao, and D. Poulikakos, "An experimental study of molten microdroplet surface deposition and solidification: Transient behavior and wetting angle dynamics," *ASME J. Heat Transfer* **122**, 544 (2000).
- ¹⁸*Handbook of Chemistry and Physics*, edited by D. R. Lide (Chapman & Hall/CRC Press, Cleveland, 2001).
- ¹⁹T. E. Faber, *Fluid Dynamics for Physicists* (Cambridge University Press, New York, 1995).
- ²⁰P. Marmottant, M. Versluis, N. d. Jong, S. Hilgenfeldt, and D. Lohse, "High-speed imaging of an ultrasound-driven bubble in contact with a wall: 'Narcissus' effect and resolved acoustic streaming," *Exp. Fluids* **41**, 147 (2006).
- ²¹P. K. Kundu and I. M. Cohen, *Fluid Mechanics* (Academic, San Diego, 2002).
- ²²M. Abramowitz and I. A. Stegun, *Handbook of Mathematical Functions with Formulas, Graphs, and Mathematical Tables* (John Wiley, New York, 1985).
- ²³T. Insperger and G. Stepan, "Stability of the damped Mathieu equation with time delay," *J. Dyn. Syst., Meas., Control* **125**, 166 (2003).